Received 13 December 2021; revised 26 January 2022; accepted 27 February 2022. Date of publication 28 March 2022; date of current version 7 April 2022.

Digital Object Identifier 10.1109/JMW.2022.3155793

Structured-Glass Waveguide Technology for High-Performance Millimetre-Wave Components and Systems

CHAD BARTLETT [1] (Student Member, IEEE), ANTONIO MALAVÉ [2], MARTIN LETZ [3], AND MICHAEL HÖFT [1] (Senior Member, IEEE)

(Regular Paper)

[1] Institute of Electrical and Information Engineering, University of Kiel, 24143 Kiel, Germany
[2] Institute for Materials Science, University of Kiel, 24143 Kiel, Germany
[3] Research and Technology Development Department, Schott, AG 55122 Mainz, Germany

CORRESPONDING AUTHOR: Chad Bartlett (e-mail: chb@tf.uni-kiel.de).

This work was supported in part by the European Union's Horizon 2020 Research and Innovation Programme under the Marie Skłodowska-Curie Grant 811232-H2020-MSCA-ITN-2018 and in part by the DFG Open Access Publication Funding Programme of Kiel University.

ABSTRACT This work presents a novel waveguide medium based on laser-induced structured-glass for the design of high-end millimetre-wave components and systems. The material properties, fabrication process and functional attributes of the structured-glass technology are first described and then applied in order to demonstrate a fourth-order bandpass filter prototype operating within the W-band frequency range, centered around 88 GHz with a narrow fractional bandwidth of 2.3%. The basic filter design, dimensional considerations, and assembly process are discussed in order to outline the fabrication process. The prototype filter, along with its associated feed-line transitions and split-block interface are measured and characterized in the laboratory in order to validate the design approach. The measured response is shown to be exceptionally accurate; the insertion loss is found to be approximately 1.43 dB - 1.97 dB throughout the measured passband with a return loss of better than 22 dB and center-frequency offset of approximately 0.117%. A comparison to existing technologies is discussed in order to highlight the advantages of the proposed medium and to contrast the differences in both manufacture and achievable results for high-end components.

INDEX TERMS Bandpass filter, laser-induced micromachining, microfabrication, millimetre-wave, passive components, structured glass, waveguide technology, W-band.

I. INTRODUCTION

Waveguide components are an integral part of high-end radar, broadcasting, satellite, and communication systems. This technology plays an important role as a transmission and signal-control medium in the form of devices such as filters and couplers, and allows for versatile designs that are capable of handling high-power and maintaining low losses in vital information systems.

For waveguide-based components manufactured in conventional alloys, traditional methods such as computer numerical control (CNC) milling and electric discharge machining (EDM) have been at the forefront of production due to their high reliability and straightforward fabrication procedures. However, the application of additive manufacturing technologies such as selective-laser-melting (SLM) and selective-laser-sintering (SLS) are under intense research due to their foreseen potential in complex and scalable manufacturing scenarios (e.g. [1]–[5]). Although CNC and EDM fabricated components have been able to demonstrate good results and are well adopted by industry, drawbacks such as cost, yield, and production volume are difficult to overcome for ever-changing global markets and have given rise to competitive solutions provided by the alternative technologies that have been previously mentioned. Furthermore, micro-scale fabrication for applications beyond microwave frequencies require a level of precision that is difficult to reach

This work is licensed under a Creative Commons Attribution 4.0 License. For more information, see https://creativecommons.org/licenses/by/4.0/

without high-precision tools and fine metrology equipment. Approaches in the form of both additive and subtractive manufacturing have been proposed in the literature to overcome these challenges at millimetre-wave frequencies. For instance, in the W-band region (75–110 GHz), these solutions include the use of stereolithography (SLA) [6]–[9], selective laser melting (SLM) [10], selective laser sintering (SLS) [11], and micro-laser sintering (MLS) [4], [5] as technology based approaches while the use of admittance-inverter sequences have been applied in [9] as a synthesis based approach.

In regards to subtractive manufacturing processes for waveguide-based components, silicon micromachining with the deep-reactive ion etching (DRIE) process is a fabrication method that has gained much attention as a potential candidate for achieving micro-scale designs. The DRIE process allows the production of three-dimensional geometries based on multi-wafer bonding and can achieve micrometre sized features in batch production scenarios. Recent work in this field has demonstrated many components well into the 220–330 GHz region and has been also been exhibited for a wide range of waveguide and filter components throughout the millimetre and sub-millimeter wave bands; several notable examples of the technology's potential can be reviewed in [12]–[19]. However, challenges with fabrication arise - particularly at the lower end of terahertz frequencies - due to under-etching of sidewalls and problems with the subsequent metallization. These challenges can require extensive production iterations and refined nano-fabrication skills.

Other technologies such as SU-8 micromachining, hot embossing, and electroforming [20]–[26] have also been demonstrated, however, each of these aforementioned technologies pose there own inherent benefits and drawbacks, and must be selected appropriately for their end-use application. A review of the technologies that have been mentioned, including DRIE, exhibit a varying level of achievable results, and while significant attributes such as batch-production are highly desirable, can come at the expense of using materials that are much different than standard milling alloys which are generally more resistant to thermal expansion (e.i. polymers or plastics vs. brass and invar). Furthermore, as mentioned in the case of technology such as DRIE micromachining, a significant amount of time must be invested in compensating the effects of sidewall under-etching and scalloping that can shift the resonant frequency of cavities and change the coupling coefficient between resonators, which ultimately leads to considerable deviation between the desired and measured responses.

To this end, we propose and demonstrate a novel *structured-glass* based waveguide technology for future millimetre-wave components and systems based on the laser-induced-micromachining of glass wafers. The proposed fabrication method allows for the incorporation of CNC-like abilities with that of the batch production capabilities of silicon-wafer based methods. This high-precision structured-glass fabrication method is aimed to overcome challenges in the production of millimetre and sub-millimetre components or systems, especially for the case of high-end applications such as non-destructive testing, earth observation, spectroscopy, and wireless communications. The key attributes from the use of this technology for millimetre-wave components come in the form of: simple wafer processing with no chemical under-etching or side-wall scalloping effects, very low achievable surface roughness, high achievable aspect ratio and highly accurate achievable dimensions. The goal of this work is to exemplify the cumulation of these effects in the form of low loss and negligible center-frequency offset between simulated and measured results. Additionally, it is well known in industry and suitably demonstrated by [29], that a decrease in fractional bandwidth (FBW) leads to a filter's performance being more sensitive to fabrication tolerances. In this regard, we aim to further demonstrate the high-precision capabilities of the technology by electing to demonstrate a narrow-band (2.3% FBW) Chebyshev filter response within the W-band region for 88 GHz operation. In the pages that follow, Section II outlines the material properties and design considerations of laser-induced structured glass, Section III presents a fourth-order filter design with application to a structured-glass wafer profile, Section IV discusses the fabrication, assembly, and measurements, Section V compares the measured results to the state of the art, and finally, Section VI serves as conclusion.

TABLE 1. General Properties of the Structured-Glass Wafers

Glass Type	Borosilicate (Borofloat 33®) [27], [28]
Dielectric Constant ϵ_r	4.4
tanδ @(77 / 110 GHz)	0.0127 / 0.0152
Density p	2.23 g/cm^3
Young's Modulus E	64 GPa
Thermal Expansion Coefficient α (20°C; 300°C)	$3.29 \cdot 10^{-6} K^{-1}$
Transformation Temp. T_g	528°C

II. STRUCTURED GLASS TECHNOLOGY

Laser-induced micromachining of structured glass is a subtractive manufacturing process that enables micro-structures to be produced throughout silicon-based wafers. The process allows for features to be micromachined though the extent of the substrate and is able to achieve via hole aspect ratios up to 25:1 and fire-polished surface roughnesses of < 1 nm [27], [28]. With the combination of precise laser-induced micro features and standard wafer processing techniques, conventional circular and rectangular substrates with 100 mm and 200 mm cross sections can be manufactured as a batch process, allowing for many components or subsystems to be manufactured simultaneously with feature sizes as small as 30 μm. In this work, borosilicate-glass (Borofloat 33®) has been selected as the base material for wafer production using Schott's Flexinity® process [27], which has been able to demonstrate wafer processing of this type on 600 mm panels for economically scalable production. Table 1 provides the general properties of

TABLE 2. Sample Comparison of Reported High-Precision Manufacturing Capabilities

Technology	Fabrication Process	Dimensional Accuracy (μm)	Surface Roughness (nm)	Thermal Expansion Coefficient† α ($10^{-6}K^{-1}$)	Ref.
DRIE	Batch	<2	100 R_{RMS}	2.6 (Silicon)	[30]
CNC	Serial	<2	75 R_a	18.7 (Brass)	[31]
Electroforming	Batch	<1	300 R_{RMS}	16.5 (Copper)	[32]
SU-8	Batch	<2	40-50 R_{RMS}	52 (SU-8)	[33]
Micro-laser Sintering	Batch	<5*	<5000 R_a	10.8 (S.S. 17-4PH)	[4], [5]
Hot Embossing	Batch	<25	135 R_{RMS}	N/A (Plastic)	[24], [25]
Laser Micromachining	Serial	<5	1250 R_a	18.7 (Brass)	[7]
L.I. Structured Glass	Batch	<3‡	250-800 R_a (w/Au)△	3.29 (Borofloat 33®)	T.W.

†CTE of assumed base material. ‡On panel size (up to 600 mm × 600 mm) the position tolerance is +/-10 μm, on device level the dimensional accuracy can be strongly reduced based on the design. △250 nm on chip surface, 800 nm on laser-etched sidewalls. *Print-layer height with powder particle sizes < d_{80} 5 μm. L.I. = laser induced, S.S. = stainless steel.

the substrate material. Several interesting characteristics can be noted from the selection of Borofloat 33®; one being the high temperature transformation $Tg = 528°$C and the second being the thermal expansion coefficient $\alpha = 3.29 \cdot 10^{-6}K^{-1}$. In combination with the fine micromachining capabilities, this technology has the potential to overcome many production and power-limited challenges that are posed by current millimetre and sub-millimetre wave technologies. Furthermore, the selection of the structured-glass base material is not limited to Borofloat 33® and the manufacturing process can be readily applied to other substrate formulas such as MEMpax® and AF32 eco® [27].

Similar to the DRIE fabrication process, multi-wafer stacking can be applied to construct 3D structured-glass waveguide components in a double H-plane split fashion. In this manner, the middle-component layer requires a top and bottom layer to form a fully enclosed structure; Fig. 1 contrasts the double H-plane split with the commonly used (e.g. CNC milling) single H-plane split. The height of the waveguide is defined by the thickness of the glass-wafer that will be used in the center of the double H-plane split. Two additional wafers are used to realise the top and bottom of the waveguide lids and can be used as simple covers or to house additional features such as waveguide transitions. One of the main advantages of this technology over others such as DRIE micromachining, is that the fabrication process does not suffer from under-etching and scalloping of the waveguide sidewalls and can easily maintain vertical sidewalls. This under-etching and scalloping effect can change the resonator cavity and iris width/thicknesses, which ultimately detunes the component and can be both difficult and cumbersome to compensate for in the early design stages, leading to multiple production iterations. Additionally, the DRIE method can further be contrasted from the proposed structured-glass method due to the absence of a designated 'device layer,' 'handle layer,' and 'SiO_2 buried oxide layer'. A sample comparison of high-precision manufacturing capabilities that have been demonstrated in the literature can be reviewed in Table 2. The thermal expansion coefficient (CTE) of the assumed base material is also given for the consideration of high-power and temperature sensitive applications.

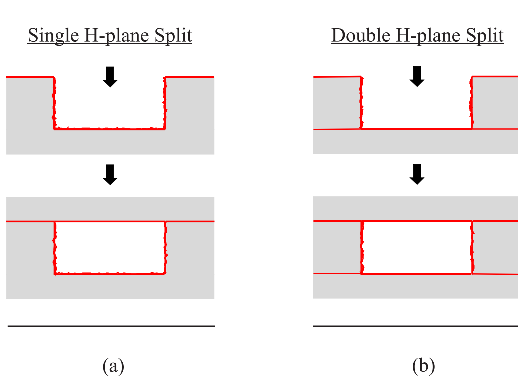

FIGURE 1. (a) A single H-plane split used in typical CNC milling for two-piece construction and (b) a double H-plane split used in alternative methods such as silicon micromachining for three-piece construction.

Once a waveguide or component fabrication profile is selected for the double H-plane split and the features are laser micromachined throughout, a metallization layer must be applied in order to mimic a metallic waveguide profile. For the case at hand, gold (Au) has been selected for its high conductivity ($\sigma \approx 45.61$ MS/m) and its well-known ability to be sputtered on glass substrates with a thin chromium (Cr) adhesion layer. In light of the straightforward process and highly accurate structured-glass profiles introduced by laser-induced micromachining, the inception of high-frequency components and subsystems can be investigated for ultra high-end or stringent applications requiring minimal insertion loss and minimal frequency offset.

III. FILTER DESIGN

In order to evaluate the technology's realizable potential for millimetre wave components, a fourth-order Chebyshev bandpass filter has been selected for narrow-band operation within the W-band region. The filter has been specified for a 2.3%

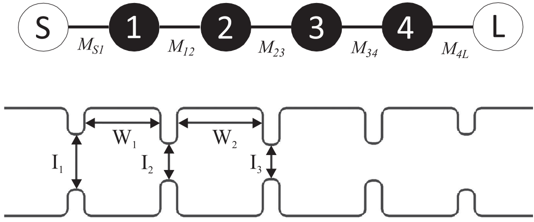

FIGURE 2. Fourth-order coupling topology (top) and cavity layout of the filter structure (bottom). Filter dimensions (rounded to three decimal places) are for the component package (optimized with transitions): $I_1 = 1281\ \mu m$, $I_2 = 847\ \mu m$, $I_3 = 785\ \mu m$, $W_1 = 1831\ \mu m$, and $W_2 = 2051\ \mu m$ with standard WR-10 waveguide ports.

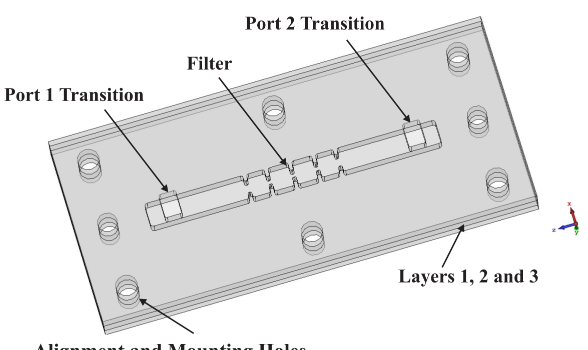

FIGURE 3. CAD layers of the proposed filter structure with the E-plane transitions ports; three wafer chips with similar heights are stacked to assemble the full component package.

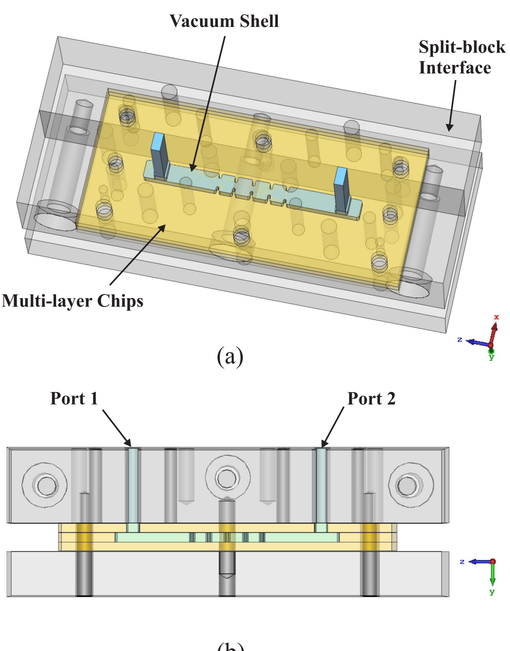

FIGURE 4. CAD model view of the metallic split-block interface and filter component package. (a) A perspective view of the assembly and (b) a front view of the assembly. Gray indicates the metallic split-block interface, orange indicates the filter component, and blue highlights the vacuum structure.

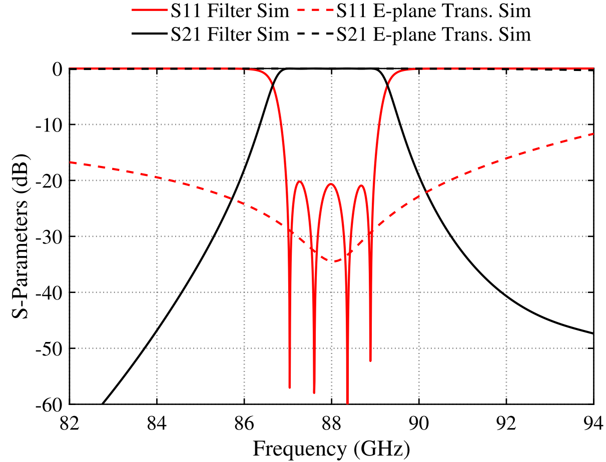

FIGURE 5. Simulated lossless S-parameters of the filter component package and of a single E-plane transition.

fractional bandwidth (FBW) at approximately 88 GHz. This narrow-band range covers approximately 2 GHz around the given center frequency and has been selected for its frequency allocation and direct application to earth-observation satellites and radio-astronomy research. The topology of the filter and its coupling scheme are shown in Fig. 2. The initial conditions for Chebyshev response is modelled from the standard equations outlined by [34], where the generalized non-zero coupling coefficients are $M_{S1} = M_{4L} = 1.0352$, $M_{12} = M_{34} = 0.9106$, and $M_{23} = 0.6999$.

Fig. 2 also presents the physical layout and dimensions which correspond to the coupling scheme specified above. The inner corner radius values are set to 0.2 mm while the outer corner radius values are set to 0.152 mm, and standard WR-10 waveguide dimensions (1.27 x 2.54 mm) are specified for the maximum height and width. In typical CNC milled designs, the filter would incorporate standard UG387/U waveguide flanges inline with the input and output of the waveguide, however, in this case, the waveguide flanges are to be situated orthogonal to the wafer body where E-plane transitions are used as a feeding mechanism. This type of wafer feeding is similar to the feeding profiles adopted in DRIE-based designs [12], [13]. Fig. 3 depicts the proposed filter structure based on three-wafer layers with E-plane port transitions. Screw-mounting holes and alignment pin holes are included through the structured-glass wafers and allow for the fully-assembled package to be mounted between split-block interfaces for final measurements and characterization. Fig. 4(a) and (b) present the full layout the system with the E-plane transitions and a custom split-block interface attached. The interface lines are 10 mm in length and high-precision milled in brass with UG387/U waveguide flanges at the feed ports. Due to the novelty of the process presented in this work, no integrated system or glass-based calibration standards have been adopted for this technology at this time and we present the filter, E-plane transitions and split-block interface as a *filter component package*, where the calibration reference

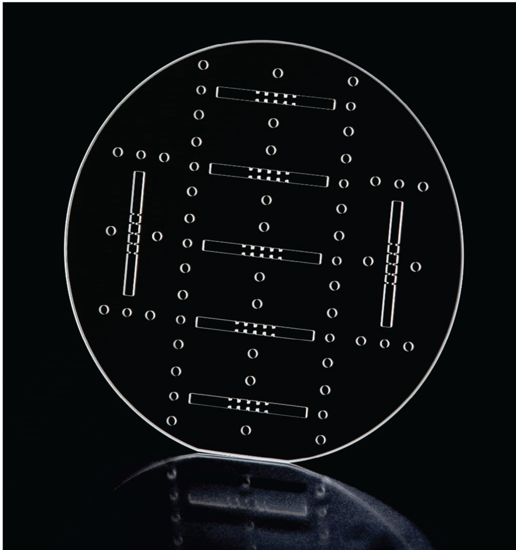

FIGURE 6. A structured-glass wafer sample (100 mm ⌀) with multiple filter structures throughout. (The sample shown is for the middle layer of the filter design shown in Fig. 3).

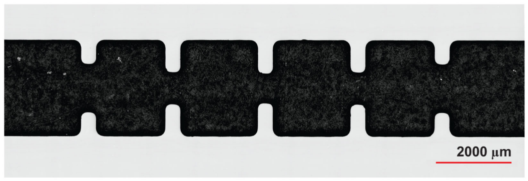

FIGURE 7. Laser-microscope view of a single laser-induced filter throughout the structured-glass wafer shown in Fig. 6.

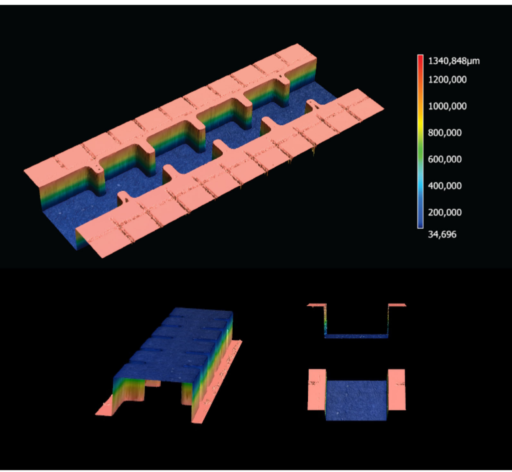

FIGURE 8. 3-D Laser-microscope profiles of the single laser-induced filter shown in Fig. 7. (Grid lines shown on top of the profile are an artifact of the microscope scan). The short waveguide sections (lower right) highlight the vertical sidewall profile at the input section of the filter.

plane is taken at the input ports of the split-block interface of Fig. 4(a) and (b). The final simulations and optimization of the filter response is carried out in CST Microwave Studio and include the effects of the E-plane transitions and split-block interface. Fig. 5 depicts the narrow-band frequency response of the simulated lossless S-parameters for the component package over 82 - 94 GHz. Additionally, the simulated frequency response of a single E-plane transition is shown in order to highlight a good return loss response within the frequencies of interest.

IV. FABRICATION AND MEASUREMENT

A. FABRICATION DETAILS

For the fabrication of the filter, three Borofloat 33® wafers are prepared using laser-induced etching. Each of the wafers serves as one of the three layers in the double H-plane split configuration, as described in Section II and applied to Fig. 3. Due to the processing of the structured glass from the manufacturer, the glass wafers are able to maintain a fine surface finish suitable for metallization by sputtering. However, it is important to note that in order to adhere to a proper skin depth ($\delta \approx 0.254$ μm at 88 GHz), the target thickness of metallization coating must be subtracted from the CAD model. In this case, we take approximately 6x the skin depth (δ) in order to allow for a high conductivity and adequate coating throughout. Each of the glass wafers has been specified for a thickness 1.267 mm. The reduction in height allows for a metallization layer of 1.5 μm on each side of the wafers. A 1.5 μm layer was also removed from sidewalls of the CAD model to account for sufficient metallization. This consideration during fabrication helps to maintain the proper final dimensions of the filter and reduces the possibility of a center-frequency offset during measurements. A structured-glass wafer sample is depicted in Fig. 6. This wafer sample is the middle layer of the component that houses the fourth-order filter design. A laser microscope was used to inspect the features and fine surface finish; Fig. 7 depicts the laser microscope view of a single laser-induced filter throughout the glass wafer. Additionally, 3-dimensional views of the filter profile are rendered from the laser microscope scans and are shown in Fig. 8. Inspection of the sidewalls at the input section of the filter (lower right images of Fig. 8) demonstrate a straight cut through the wafer, where no under-etching of the sidewalls is indicated.

Once each of the three wafers is micromachined with their respective structures and inspected, the individual wafers are diced into individual chip components for metallization and assembly. In typical silicon-micromachining and MEMs manufacturing, the full wafer is usually metallized (and sometimes bonded) before dicing, however, for this experiment, we have selected to free each of the structured-glass chips before the metallization process takes place; this was done to conserve resources while refining the fabrication, assembly, and bonding processes. To this end, the structured-glass chips are then metallized in a two stage sputtering chamber, where the first stage applies a 50 nm chromium (Cr) layer to support proper glass-to-metal adhesion, and the second stage applies 2.1 μm of gold (Au) as the the conductive layer for wave propagation. The surface roughness of the metallized chips remains on the

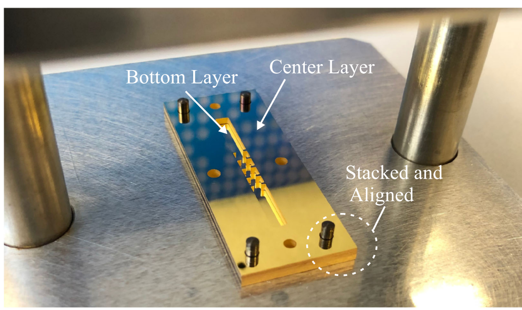

FIGURE 9. Partial assembly of the prototype; the gold (Au) sputtered bottom glass-layer chip and center glass-layer chip are stacked and aligned with high-precision pins prior to the bonding procedure. The bottom glass-layer chip can be seen clearly through the channel of the center glass-layer chip.

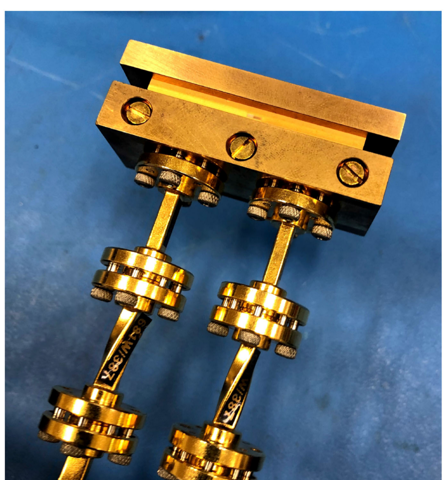

FIGURE 10. Assembled prototype and split-block interface attached to the test-bed.

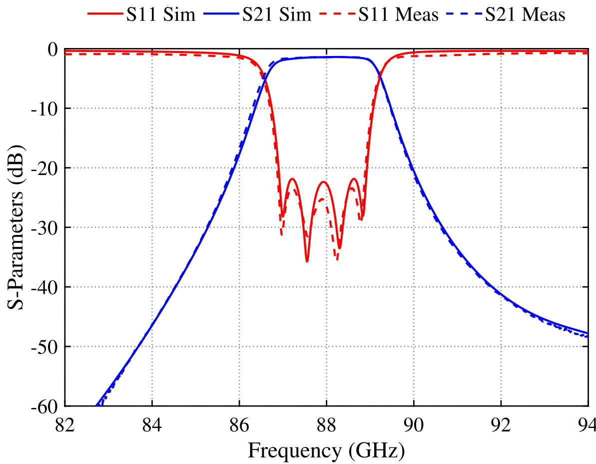

FIGURE 11. Narrow-band S-parameter response of the filter package. Equivalent conductivity taken as 2.10 MS/m.

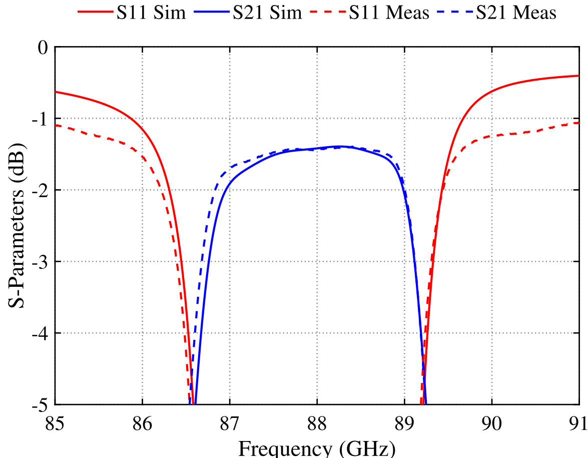

FIGURE 12. Close-up view of the S-parameter response. Equivalent conductivity taken as 2.10 MS/m.

order of approximately $S_a = 250$ nm. As previously mentioned, a 1.5 μm layer was accounted for in the sidewalls of the CAD vacuum structure, however, to ensure a sufficient and uniform metallization layer was applied within the waveguide walls, a slightly thicker value (2.1 μm) of sputtered gold (Au) was selected as a precaution.

Completion of the metallization allows for the individual chips to be inspected for errors before chip-to-chip (multi-layer) bonding. Surface roughness measurements of the gold (Au) coated chip surfaces are on the order of 250 nm, while the laser-etched side walls are on the order of 800 nm. Once cleaned and inspected, three individual chips are stacked and aligned using high-precision alignment pins and are then thermo-compression bonded at 250 $^\circ$ for 2.5 hours. During bonding, localized gaps are minimized due to the malleability of the metallization layer and aided by the fine surface finish of the glass. No additional adhesive material was applied. Fig. 9 depicts the stacking and alignment of two chip layers before the bonding process takes place. Due to the CTE of the metallization being larger than the CTE of the glass, as well as being more ductile and thinner than the glass wafer, the metallization layer will follow the glass during temperature variation and should not cause any major problems as long as adhesion during the thermos-compression bonding process was carried though effectively.

B. MEASUREMENT DETAILS

Once fabricated and assembled, the filter component package was tested using a Rohde & Schwarz ZVA67 with W-band up-converters. An image of the unit connected to the test-bed is shown in Fig. 10. The bonded glass-wafers and split-block interface can be seen clearly and resembles the CAD models of Fig. 4 closely. Fig. 11 presents a comparison of the simulated and measured results of the filter over a narrow-band range of 82 - 94 GHz. This direct comparison demonstrates excellent measured results; the measured return loss is better than 22 dB and the measured insertion loss is found to be in the range of approximately 1.43 dB–1.97 dB throughout the measured passband. High accuracy between the simulated and measured responses can be noted; the extremely small

TABLE 3. Sample Comparison of High-Precision Manufactured Filters at the W-Band Region

Technology	Center Freq. (f_o)	FBW (%)	N, Tz	IL* (dB)	RL (dB)	Center Freq. Offset (%)	Ref.
DRIE	92.45	4.83	3, 0	1.1	> 10	NA	[14]
CNC	100	10	4, 1	0.6	> 18	NA	[35]
CNC	97.5	2	6, 2	1.4	> 19.7	NA	[36]
CNC	93.0	2.1	3, 0	2.0	> 10	NA	[37]
SU-8	88.47	9.7	4, 0	0.97	> 15	1.70	[38]
SU-8	102	5	4, 2	1.2	> 10	2.00	[39]
Micro-laser Sintering	89.1	11.07	5, 0	1.0	> 15	1.0	[4]
Electroforming	95	21	10, 0	0.4	> 15	NA	[26]
Hot Embossing	96.77	3.15	5, 0	1.22	> 9.3	0.145	[25]
Thin Film Microstrip	93.8	1.3	2, 0	1.75	> 14.5	0.21	[40]
Laser Micromachining	100	4	4, 0	0.65	> 15	NA	[7]
L.I. Structured Glass	87.86	2.3	4, 0	1.43	> 22	0.117	T.W.**

Table values are estimated as best as possible for the presented measured data where not directly reported. *Measured data is reported as the achieved typical value, minimum achieved value, or at center frequency (rather than a range), **Filter includes E-plane transitions and split-block interface. L.I. = laser induced, N = number of poles, Tz = number of transmission zeros.

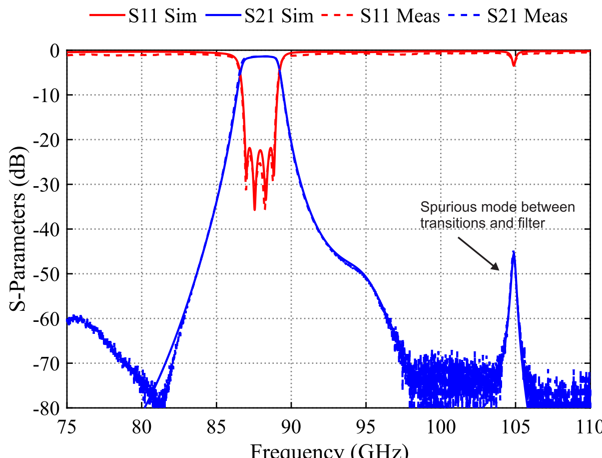

FIGURE 13. Full-band S-parameter response of the filter package. Equivalent conductivity taken as 2.10 MS/m.

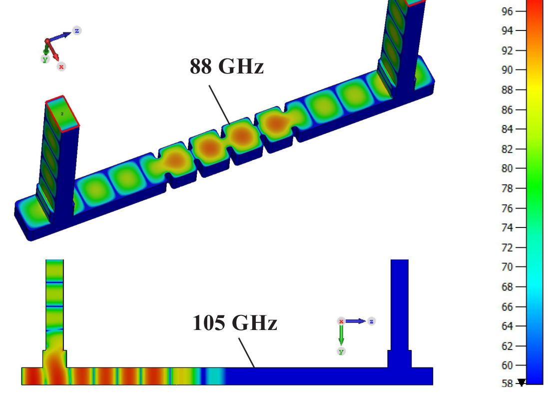

FIGURE 14. Electromagnetic field distributions of the filter component package at 88 GHz (passband) and along the half-cut YZ-plane at 105 GHz (spurious mode).

offset between the measured and simulated center frequency locations is found to be approximately 0.117 %. The unloaded quality factor of the filter package (with the transitions and split-block interface included) is estimated to be approximately $Q_u \approx 570$.

A close-up view of the insertion loss is depicted in Fig. 12 for the range of 85–91 GHz, while the full-band response of the filter is depicted in Fig. 13 from 75–110 GHz. Minor deviation can be shown between the simulated and measured results and is attributed to micro-misalignments as well as the use of the split-block interface. It can also be noted that there is a very accurate agreement between the measurement and simulation throughout the full-band response shown in Fig. 13. A spurious mode can be observed at approximately 105 GHz. This spurious response is stimulated between the E-plane transitions and the filter. However, this spurious mode remains below −40 dB and can be disregarded once the technology is advanced enough to be calibrated with integrated glass standards or later part of an isolated system, which will also simultaneously improve the small deviations between the simulated and measured results and increase the overall Q-factor. For the readers interest, Fig. 14 is given in order to highlight the electromagnetic field distributions of the filter package at 88 GHz (in the passband) and along the half-cut YZ-plane at 105 GHz (the spurious mode).

V. LITERATURE COMPARISON

Table 3 has been provided as a sample comparison of existing high-performance filter technologies at the W-band region. A comparison can be made between fabrication technologies

and reported results, allowing for the structured-glass waveguide filter to be assessed for the first time in the literature. As can be observed in Table 3 and upon review of Fig. 13, the accuracy of the return loss response and minimal offset in measured center frequency is exceptional; > 22 dB and ≈ 0.117 %, respectively. It can be noted that the results are highly competitive with the other existing technologies, especially in the case of sampled filters that demonstrate a narrow FBW and with the consideration that the measurements of this work include the lossy effects of the E-plane transitions and split-block interface. Additionally, Table 2 has been provided as a comparison of achievable results with precision manufacturing, where notably, the CTE of Borofloat 33® structured glass is low ($\alpha = 3.29 \cdot 10^{-6} K^{-1}$). This comparison establishes laser-induced structured glass as a viable candidate for future millimetre-wave designs and demonstrates the high-precision capabilities of the technology for high-performance requirements.

VI. CONCLUSION

A novel waveguide medium for the design of millimetre-wave components and systems based on laser-induced structured glass has been proposed. A presentation on the design aspects and fabrication process has been discussed and applied to the prototyping of a fourth-order Chebyshev bandpass filter operating within the W-band. Measurements of the filter prototype have demonstrated highly accurate results throughout the measured region of interest, allowing for the proposed method of manufacture to be verified experimentally. Verification of this work allows for a novel research branch to be investigated with the aim of overcoming challenges within the millimetre-wave bands and can promote further exploration into the sub-millimetre-wave bands. Furthermore, future work in this field can be applied to both passive and active circuits, front-end systems, antennas, and circuit transitions (e.g. microstrip-to-waveguide). The assembly process is universal, and therefore multi-layer or surface mounted components can be expanded for larger glass-based integrated modules and subsystems, allowing for new interdisciplinary research and novel commercial applications in future works.

REFERENCES

[1] R. V. Snyder, G. Macchiarella, S. Bastioli, and C. Tomassoni, “Emerging trends in techniques and technology as applied to filter design,” *IEEE J. Microwaves*, vol. 1, no. 1, pp. 317–344, Jan. 2021.

[2] C. Tomassoni, O. A. Peverini, G. Venanzoni, G. Addamo, F. Paonessa, and G. Virone, “3-D printing of microwave and millimeter-wave filters: Additive manufacturing technologies applied in the development of high-performance filters with novel topologies,” *IEEE Microw. Mag.*, vol. 21, no. 6, pp. 24–45, Jun. 2020.

[3] O. A. Peverini *et al.*, “Selective laser melting manufacturing of microwave waveguide devices,” *Proc. IEEE IRE*, vol. 105, no. 4, pp. 620–631, Apr. 2017.

[4] M. Salek *et al.*, “W-band waveguide bandpass filters fabricated by micro laser sintering,” *IEEE Trans. Circuits Syst. II, Exp. Briefs*, vol. 66, no. 1, pp. 61–65, Jan. 2019.

[5] M. Salek *et al.*, “90 GHz micro laser sintered filter: Reproducibility and quality assessment,” in *Proc. 49th Eur. Microw. Conf.*, Paris, France, 2019, pp. 296–299.

[6] M. D’Auria *et al.*, “3-D printed metal-pipe rectangular waveguides,” *IEEE Trans. Compon. Packag. Manuf. Technol.*, vol. 5, no. 9, pp. 1339–1349, Sep. 2015.

[7] X. Shang *et al.*, “*W*-band waveguide filters fabricated by laser micromachining and 3-D printing,” *IEEE Trans. Microw. Theory Techn.*, vol. 64, no. 8, pp. 2572–2580, Aug. 2016.

[8] C. Guo *et al.*, “Novel microwave/millimeter-wave passive waveguide devices based on 3-D printing techniques,” *J. Infrared Millimeter THz Waves*, vol. 36, no. 1, pp. 81–91, 2017.

[9] C. Bartlett, J. Bornemann, and M. Höft, “3D-Printing and high-precision milling of W-band filter components with admittance inverter sequences,” *IEEE Trans. Compon. Packag. Manuf. Technol.*, vol. 11, no. 12, pp. 2140–2147, Dec. 2021.

[10] B. Zhang and H. Zirath, “3-D printed Iris bandpass filters for millimetre-wave applications,” *IET Electron. Lett.*, vol. 51, no. 22, pp. 1791–1793, 2015.

[11] R. Fujiwara *et al.*, “3-D printed Iris waveguide filter in W-band,” in *Proc. 23rd Int. Microw. Radar Conf.*, Warsaw, Poland, 2020, pp. 346–349.

[12] X. Zhao *et al.*, “Silicon micromachined D-band diplexer using releasable filling structure technique,” *IEEE Trans. Microw. Theory Techn.*, vol. 68, no. 8, pp. 3448–3460, Aug. 2020.

[13] J. Campion *et al.*, “An ultra low-loss silicon-micromachined waveguide filter for D-band telecommunication applications,” in *Proc. IEEE MTT-S Int. Microw. Symp.*, 2018, pp. 583–586.

[14] Y. Li, P. L. Kirby, and J. Papapolymerou, “Silicon micromachined W-band bandpass filter using DRIE technique,” in *Proc. 32nd Eur. Microw. Conf.*, Manchester, U.K., 2006, pp. 1271–1273.

[15] J.-X. Zhuang, Z.-C. Hao, and W. Hong, “Silicon micromachined terahertz bandpass filter with elliptic cavities,” *IEEE Trans. THz Sci. Technol.*, vol. 5, no. 6, pp. 1040–1047, Nov. 2015.

[16] C. A. Leal-Sevillano *et al.*, “Silicon micromachined canonical E-plane and H-plane bandpass filters at the terahertz band,” *IEEE Microw. Wireless Compon. Lett.*, vol. 23, no. 6, pp. 288–290, Jun. 2013.

[17] O. Glubokov, X. Zhao, J. Campion, U. Shah, and J. Oberhammer, “Micromachined bandpass filters with enhanced stopband performance and Q-factor of 950 at 700 GHz,” in *Proc. IEEE MTT-S Int. Microw. Symp.*, Atlanta, GA, USA, 2021, pp. 204–206.

[18] O. Glubokov, X. Zhao, B. Beuerle, J. Campion, U. Shah, and J. Oberhammer, “Micromachined multilayer bandpass filter at 270 GHz using dual-mode circular cavities,” in *Proc. IEEE MTT-S Int. Microw. Symp.*, 2017, pp. 1449–1452.

[19] C. Jung-Kubiak *et al.*, “A multistep DRIE process for complex terahertz waveguide components,” *IEEE Trans. THz Sci. Technol.*, vol. 6, no. 5, pp. 690–695, Sep. 2016.

[20] X. Shang, M. Ke, Y. Wang, and M. J. Lancaster, “WR-3 band waveguides and filters fabricated using SU8 photoresist micromachining technology,” *IEEE Trans. THz Sci. Technol.*, vol. 2, no. 6, pp. 629–637, Oct. 2012.

[21] X. Shang, H. Yang, Y. Dhayalan, M. J. Lancaster, H. Wang, and P. G. Huggard, “SU-8 micromachined cross-coupled waveguide cavity filter for sideband rejection above 300 GHz,” in *Proc. 10th U.K.-Eur.-China Workshop mm-Waves THz Technol.*, Liverpool, U.K., 2017, pp. 1–2.

[22] Q. Chen, X. Shang, Y. Tian, J. Xu, and M. Lancaster, “SU-8 micromachined WR-3 band waveguide bandpass filter with low insertion loss,” *IET Electron. Lett.*, vol. 49, no. 7, pp. 480–482, Mar. 2013.

[23] X. Shang, H. Yang, D. Glynn, and M. J. Lancaster, “Submillimeter-wave waveguide filters fabricated by SU-8 process and laser micromachining,” *IET Microw. Antennas Propag.*, vol. 11, no. 14, pp. 2027–2034, Oct. 2017.

[24] F. Sammoura *et al.*, “A micromachined W-band Iris filter,” in *13th Int. Conf. Solid-State Sensors Actuators Microsys Dig. Technol.*, 2005, pp. 1067–1070.

[25] F. Sammoura *et al.*, “Plastic 95-GHz rectangular waveguides by micro molding technologies,” *Sensors Actuators Phys.*, vol. 127, pp. 270–275, Mar. 2006.

[26] C. A. Leal-Sevillano *et al.*, "Development of low loss waveguide filters for radio-astronomy applications, infra," *Phys. Techn.*, vol. 61, pp. 224–229, Nov. 2013.
[27] SCHOTT, "Glass made of ideas," Flexinity. Accessed: Oct. 29, 2021. [Online]. Available: https://www.schott.com/de-de/products/flexinity-p1000320
[28] M. Letz *et al.*, "Special glass for packaging of high frequency electronics," in *Proc. 51st Eur. Microw. Conf.*, to be published, 2021.
[29] J. Bornemann, U. Rosenberg, S. Amari, and R. Vahldieck, "Tolerance analysis of bypass-, cross-, and direct-coupled rectangular waveguide band-pass filters," *IEEE Proc. Microw., Antennas Propag.*, vol. 152, no. 3, pp. 167–170, Jun. 2005.
[30] T. Reck *et al.*, "Silicon micromachined waveguide components at 0.75 to 1.1 THz," in *Proc. 39th Int. Conf. Infrared Millimeter THz Waves*, Tucson, AZ, USA, 2014, pp. 1–2.
[31] C. Groppi *et al.*, "Automated CNC micromachining for integrated THz waveguide circuits," in *Proc. 21st Int. Symp. Space THz Technol.*, Oxford, U.K., 2010, pp. 338–341.
[32] F. Mena *et al.*, "RF performance of a 600–720 GHz sideband-separating mixer with all-copper micromachined waveguide mixer block," in *Proc. 19th Int. Symp. Space THz Techn.*, Groningen, The Netherlands, 2008, pp. 90–92.
[33] Y. Wang, M. Ke, M. J. Lancaster, and J. Chen, "Micromachined 300-GHz SU-8-based slotted waveguide antenna," *IEEE Antennas Wireless Propag. Lett.*, vol. 10, pp. 573–576, May. 2011.
[34] J.-S. Hong and M. J. Lancaster, *Microstrip Filters for RF/Microwave Applications*. New York, NY, USA: Wiley, 2001.
[35] C. A. Leal-Sevillano, J. R. Montejo-Garai, J. A. Ruiz-Cruz, and J. M. Rebollar, "Low-loss elliptical response filter at 100 GHz," *IEEE Microw. Wireless Compon. Lett.*, vol. 22, no. 9, pp. 459–461, Sep. 2012.
[36] C. Bartlett and M. Höft, "W-band TE102-mode filter with doubly loaded E-plane and H-plane irises," *IET Electron. Lett.*, vol. 57, no. 4, pp. 190–192, Feb. 2021.
[37] W. J. Wu, R. Zhang, and X. X. Fan, "A high stop-band suppression W-band waveguide E-plane filter for millimeter-wave applications," *IEEE Int. Conf. Microw. mm-Wave Technol.*, Beijing, China, 2016, pp. 798–800.
[38] X. Shang, M. Ke, Y. Wang, and M. Lancaster, "Micromachined W-band waveguide and filter with two embedded H-plane bends," *IET Microw. Antennas Propag.*, vol. 5, no. 3, pp. 334–339, 2011.
[39] C. A. Leal-Sevillano *et al.*, "A pseudo-elliptical response filter at W-band fabricated with thick SU-8 photo-resist technology," *IEEE Microw. Wireless Compon. Lett.*, vol. 22, no. 3, pp. 105–107, Mar. 2012.
[40] S. Song and K.-S. Seo, "A W-band air-cavity filter integrated on a thin-film substrate," *Microw. Wireless Compon. Lett.*, vol. 19, no. 4, pp. 200–202, Mar. 2009.

CHAD BARTLETT (Student Member, IEEE) was born in Nelson, BC, Canada, in 1987. He received the B.Eng. and M.A.Sc. degrees in electrical engineering from the University of Victoria, Victoria, BC, Canada, in 2017 and 2019, respectively. He is currently working toward the Dr.-Ing. degree with the Chair of Microwave Engineering, Institute of Electrical and Information Engineering, University of Kiel, Kiel, Germany. He is a member of the European Union's Horizon 2020 Research and Innovation Programme for early-stage researchers. His primary research interests include microwave and millimeter-wave passive components, filters and antenna networks for the next generation of satellite and communication systems, and developing methods for overcoming challenges in micro-scale designs.

ANTONIO MALAVÉ received the degree in physics from the University of Granada, Granada, Spain, and the Ph.D. degree in physics from the University of Kassel, Kassel, Germany, in 2004, for his work on probes for scanning force microscopy based on polycristalline diamond. In 1993, he was with the University of Málaga, Málaga, Spain, as an Associated Professor for two years. He is currently a Staff Scientist with the University of Kiel, Kiel, Germany. From 2002 to 2007, he was with the Center of Advanced European Studies and Research (caesar), Bonn, Germany, focussed on chip design and fabrication of biosensors. In 2008, he joined the Inorganic Functional Materials Group, University of Kiel, Kiel, Germany, and in 2009 responsible for the cleanroom facility in the Kiel Nanolaboratory. His main research interests include sensors and thin film deposition and patterning technologies.

MARTIN LETZ received the Ph.D. degree in solid state physics from the University of Stuttgart, Stuttgart, Germany. He is currently with SCHOTT, a special glass company, as a Senior Principal Scientist with Central R&D. In 2001, he joined SCHOTT, and was involved in several projects regarding materials for semiconductor structuring. For several years, he has been focusing on glasses and glass ceramics for electronic applications and their properties. His research interests include materials for antenna and filter structures for wireless data transfer and miniaturization of high frequency electronics. He had several positions in research institutions and Universities, such as the Tartu University, Estonia, Max-Plack Institut, Stuttgart, Germany, Queens University, Kingston, ON, Canada, and University of Mainz, Mainz, Germany, worked on different aspects of strong correlations in condensed matter.

MICHAEL HÖFT (Senior Member, IEEE) was born in Lübeck, Germany, in 1972. He received the Dipl.-Ing. degree in electrical engineering, and the Dr.-Ing. degree from the Hamburg University of Technology, Hamburg, Germany, in 1997 and 2002, respectively. From 2002 to 2013, he was with the Communications Laboratory, European Technology Center, Panasonic Industrial Devices Europe GmbH, Lüneburg. He was a Research Engineer and then the Team Leader, where he was engaged in research and development of microwave circuitry and components, particularly filters for cellular radio communications. From 2010 to 2013, he was the Group Leader of research and development of sensor and network devices. Since October 2013, he has been a Full Professor with the Faculty of Engineering, University of Kiel, Kiel, Germany, where he is currently the Head of the Chair of Microwave Engineering, Institute of Electrical and Information Engineering. His research interests include active and passive microwave components, submillimeter-wave quasioptical techniques and circuitry, microwave and field measurement techniques, microwave filters, microwave sensors, and magnetic field sensors. He is a member of the European Microwave Association (EuMA), the Association of German Engineers (VDI), and the German Institute of Electrical Engineers (VDE).